http://dx.doi.org/10.1063/1.4848856

The effect of neutrally buoyant finite-size particles on channel flows in the laminar-turbulent transition regime

Vincent Loisel,[1,2] Micheline Abbas,[1,2,a)] Olivier Masbernat,[1,2] and Eric Climent[2,3]
[1]*Université de Toulouse INPT-UPS: Laboratoire de Genie Chimique, Toulouse, France*
[2]*CNRS, Federation de recherche FERMaT, Toulouse, France*
[3]*Université de Toulouse INPT-UPS: Institut de Mécanique des fluides de Toulouse, France*

The presence of finite-size particles in a channel flow close to the laminar-turbulent transition is simulated with the Force Coupling Method which allows two-way coupling with the flow dynamics. Spherical particles with channel height-to-particle diameter ratio of 16 are initially randomly seeded in a fluctuating flow above the critical Reynolds number corresponding to single phase flow relaminarization. When steady-state is reached, the particle volume fraction is homogeneously distributed in the channel cross-section ($\phi \cong 5\%$) except in the near-wall region where it is larger due to inertia-driven migration. Turbulence statistics (intensity of velocity fluctuations, small-scale vortical structures, wall shear stress) calculated in the fully coupled two-phase flow simulations are compared to single-phase flow data in the transition regime. It is observed that particles increase the transverse r.m.s. flow velocity fluctuations and they break down the flow coherent structures into smaller, more numerous and sustained eddies, preventing the flow to relaminarize at the single-phase critical Reynolds number. When the Reynolds number is further decreased and the suspension flow becomes laminar, the wall friction coefficient recovers the evolution of the laminar single-phase law provided that the suspension viscosity is used in the Reynolds number definition. The residual velocity fluctuations in the suspension correspond to a regime of particulate shear-induced agitation.

I. INTRODUCTION

The properties of a suspension flow may be different from that of the particle-free flow. These properties depend on many parameters which can be combined under the form of dimensionless numbers as the Reynolds, Stokes, and Péclet numbers, particle-to-fluid density ratio, particle-to-channel size ratio, particle volumetric concentration, etc. In transport applications, it is of particular interest to understand how particles modulate the laminar-turbulent transition in pipe flows. It is often better to avoid operating within this regime due to unsteady large-scale structures that may develop, leading to serious equipment damages. Also, a fundamental understanding of particle-laden flows response close to the onset of turbulence is still lacking.

This paper aims at studying the effect of neutrally buoyant and finite-size particles on a channel flow close to laminar-turbulent transition. The particles considered here are non-Brownian (high Péclet number based on the ratio of the velocity perturbation at the scale of the particle multiplied by the particle diameter and the particle diffusion coefficient) and weakly inertial, i.e., their relaxation time scale in response to local flow perturbations is small (moderate Stokes number). In this case, the suspension dynamics is only a function of the channel Reynolds number, the solid volume fraction, and the particle-to-channel size ratio (or equivalently to the particle Reynolds number).

[a)]Electronic mail: Micheline.Abbas@ensiacet.fr

In the limit of highly dilute suspensions, particle dilute-induced local velocity perturbations are characterized by the local shear rate at the particle scale. In Stokes channel flow, neutrally buoyant particles follow the fluid streamlines, slightly lagging the laminar Poiseuille flow (Faxén correction), and when fluid inertia is finite, particles are submitted to lateral migration due to their interaction with the curved velocity profile.[1,2] The larger are the Reynolds number and the particle size, the faster is the migration process. When the suspension concentration is not negligible (solid volume fraction $\phi \geq 1\%$), shear-induced particle interactions generate chaotic motions of the particles and in an unbounded sheared Stokes flow it has been shown that shear-induced agitation and self-diffusion are increasing functions of the particle size, shear rate, and particle volumetric concentration.[3,4] In pressure-driven concentrated suspension flows, particles migrate towards the center of the channel at low Reynolds numbers.[5,6] However at finite Reynolds number flows in a pipe, Han *et al.*[7] have shown that preferential concentrations take place at different locations in the tube cross-section, depending strongly on the average solid volume fraction.

In turbulent suspension flows, the stochastic nature of the carrying fluid flow and the dispersed phase distribution make the problem far more complex than in laminar regime. Finite-size particles can modulate the carrier flow properties via some extra mechanisms like turbulence production, distortion and dissipation, reducing or increasing the turbulent stresses. These mechanisms depend, in addition to the particle size with respect to the smallest spatial flow scales, on the solid volume fraction as well. For more details on this topic, the reader is referred to the review of Balachandar and Eaton.[8]

A channel or pipe flow in the transition regime is usually characterized by large unsteady structures generating strong fluctuations of the local stresses. In the case of single phase flow, the critical Reynolds number below which the turbulence completely vanishes depends on the channel cross-section geometry and on the wall surface condition (as the wall roughness). Matas, Morris, and Guazzelli[9] have shown that neutrally buoyant finite-size particles can increase or decrease the critical Reynolds number depending on the particle-to-pipe diameter ratio and on the particle volumetric concentration. Their results are based on measurements of the instantaneous pressure drop along the pipe, from which the laminar-turbulent transition is detected. However, local scale interactions between the particles and the flow at the boundary of the laminar-turbulent transition were not investigated. Only recently Yu *et al.*[10] performed numerical simulations (using the Fictitious Domain Method) of a transitional pipe flow laden with large neutrally buoyant particles. For their study, the authors placed the particles in a laminar flow and considered that the transition to turbulence occurs when the fluctuating energy in time exceeds a threshold value. They confirmed that large particles trigger the transition at low particle volume fractions in agreement with the experimental observations.

We use numerical simulations in order to investigate finite-size particle-fluid interactions when the base flow undergoes a transitional regime. Thanks to the increasing availability and power of actual computational resources, resolved numerical simulations of turbulent particle-laden flows are continuously improving.[11–15] The numerical method chosen for this work fully resolves the fluid equations at a length-scale smaller than the particle radius. The numerical results are used to obtain information about the modification of the suspension flow properties compared to the single phase flow undergoing laminar-turbulent transition.

In both single and two-phase flow simulations, we use a unique definition of the Reynolds number $Re = \frac{\langle U \rangle H}{\nu}$ based on the channel height H, the average flow velocity $\langle U \rangle$, and the kinematic viscosity ν of the carrier fluid.

The paper is organized as follows: Sec. II describes the numerical method and its validation on basic cases that are representative of the studied problem. Simulation procedure is detailed in Sec. III. Section IV presents an overview on the single-phase flow behavior in the transition regime obtained from relaminarization of an initially turbulent flow. Afterwards, Sec. V shows the effect of neutrally buoyant particles on the transitional flow. The particles are large, i.e., channel height-to-particle diameter ratio is $H/d = 16$ and the suspension is moderately concentrated ($\phi = 5\%$). In this case, the turbulence of the suspension flow is expected to be sustained down to lower Reynolds numbers than that observed in single-phase flow case (Matas, Morris, and Guazzelli[9]). Section VI describes

the suspension dynamics below the transition threshold. At the end of the paper, main findings are summarized in the concluding section (Sec. VII).

II. NUMERICAL METHOD AND VALIDATION

Direct numerical simulations of single-phase flows have been performed using the code JADIM for a Newtonian incompressible fluid.[16] The Navier-Stokes equations discretized on a staggered Eulerian grid are integrated in space using a finite-volume method. All the terms involved in the balance equations are discretized using second order centered schemes in space. The solution is advanced in time by a second order Runge-Kutta time-stepping procedure and incompressibility is achieved by a corrective pressure which is solution of the Poisson equation. The exponential increase of the energy of a 2D small-amplitude disturbance in a plane Poiseuille flow has been validated following Calmet and Magnaudet.[16]

The chosen numerical approach to simulate particle trajectories and suspension flow field is based on a multipole expansion of momentum source terms added to the Navier-Stokes equations. This method is called the Force-Coupling Method (FCM). Flow equations are dynamically coupled to Lagrangian tracking of particles. The method is described in details in Maxey and Patel,[17] Lomholt and Maxey,[18] and Climent and Maxey.[19] The fluid is assumed to fill the entire simulation domain, including the volume occupied by the particles. The fluid velocity and pressure fields are solutions of the mass and momentum conservation equations (Eqs. (1) and (2)),

$$\nabla \cdot \mathbf{u} = 0, \tag{1}$$

$$\rho \frac{\mathrm{D}\mathbf{u}}{\mathrm{D}t} = -\nabla p + \mu \nabla^2 \mathbf{u} + \mathbf{f}(\mathbf{x}, t), \tag{2}$$

ρ and μ stand, respectively, for the density and the dynamic viscosity, and $\mathbf{u}$ represents the velocity vector.

The presence of the dispersed phase in the fluid is then represented by a body force distribution $\mathbf{f}(\mathbf{x}, t)$ written as a multipole expansion (Eq. (3)) where the first term is the monopole $\mathbf{F}^{(n)}$ representing the force that the nth particle applies on the fluid (due to an external forcing or particle-to-particle contact forces). The second term is the dipole $\mathbf{G}^{(n)}$ tensor. Its anti-symmetric part is related to external torques applied on the particle. The symmetric part is set through an iterative procedure to ensure that the strain-rate within the fluid volume occupied by the dispersed phase is zero (enforcing solid body response),

$$\begin{aligned} \mathrm{f}_i(\mathbf{x}, t) = &\sum_{n=1}^{N} F_i^{(n)} \Delta\left(\mathbf{x} - \mathbf{Y}^{(n)}(t)\right) \\ &+ G_{ij}^{(n)} \frac{\partial}{\partial x_j} \Delta'\left(\mathbf{x} - \mathbf{Y}^{(n)}(t)\right), \end{aligned} \tag{3}$$

$\mathbf{Y}^{(n)}$ is the nth particle center position. $\Delta(\mathbf{x} - \mathbf{Y}^{(n)})$ and $\Delta'(\mathbf{x} - \mathbf{Y}^{(n)})$, the spatial distributions of the monopole and dipole forcing, are generated using finite size envelopes that are adapted to the shape of the spherical particle. The particle translation and rotation velocities $\mathbf{V}^{(n)}$ and $\mathbf{\Omega}^{(n)}$ are obtained from a local weighted average of the volumetric fluid velocity (respectively, rotational velocity) field over the region occupied by the particle in Eq. (4) (respectively, Eq. (5)),

$$\mathbf{V}^{(n)} = \int \mathbf{u}(\mathbf{x}, t)\, \Delta(\mathbf{x} - \mathbf{Y}^{(n)})\, \mathrm{d}^3\mathbf{x}, \tag{4}$$

$$\mathbf{\Omega}^{(n)} = \frac{1}{2} \int [\nabla \times \mathbf{u}(\mathbf{x}, t)]\, \Delta'(\mathbf{x} - \mathbf{Y}^{(n)})\, \mathrm{d}^3\mathbf{x}. \tag{5}$$

Isotropic Gaussian envelopes are used for spherical particles. The respective width of these Gaussian envelopes (σ and $\sigma\prime$) is set with respect to the particle radius in such a way that the Stokes settling velocity and the hydrodynamic perturbation generated by a particle in a shear flow are both accurately reproduced at low Reynolds numbers.[18] This ensures, among other results, that the particle velocity matches the Stokes settling velocity under low particulate Reynolds number and captures the Faxén correction for the motion in a non-uniform flow.[17] Particle trajectories are then obtained from numerical integration of Eq. (6),

$$\frac{\mathrm{d}\mathbf{Y}^{(n)}}{\mathrm{d}t} = \mathbf{V}^{(n)}. \tag{6}$$

The key point of this modelling approach is that it allows calculating the hydrodynamic interactions with a moderate computational cost. In order to capture correctly the dynamics of dilute suspension flows, four grid points per particle radius are usually used when the monopole force is not zero, and in the case where only dipole forcing is relevant, three grid points per particle radius are sufficient.

When the particle volume fraction reaches a few percent, pairwise short-range hydrodynamic interactions and rigid body contact forces need to be accounted for. This is done by adding a monopole term following Abbas *et al.*,[4] which prevents particles from overlapping. The repulsive contact force between a pair of particles (α) and (β) is written as a function of the relative position vector $\mathbf{x}^{\alpha\beta} = \mathbf{Y}^{(\alpha)} - \mathbf{Y}^{(\beta)}$ and the distance $r^{\alpha\beta} = \left|\mathbf{x}^{\alpha\beta}\right|$. If $r^{\alpha\beta} < R_{ref}$ (the cut-off length scale for the barrier), then the contact force acting on particle α due to particle β, scaled by F_{ref}, reads

$$\mathbf{F}_c^{\alpha\beta} = \frac{F_{ref}}{2a}\left[\frac{R_{ref}^2 - r^{\alpha\beta^2}}{R_{ref}^2 - 4a^2}\right]^2 \mathbf{x}^{\alpha\beta}. \tag{7}$$

Otherwise the contact force is zero. In the present simulations, the value of the scaling factor F_{ref} is chosen so that the number of overlapping particles is less than one percent of the total particle number. The dynamics of the suspension flows shown in this work is not sensitive to the value of the force scale in a rather large range of variation of F_{ref}.

In the absence of external forces (no gravity effect for neutrally buoyant particles), the coupling between the particles and the carrier flow occurs exclusively from the force dipole term which is mainly related to the local flow strain rate. Accordingly, the method has been validated in finite Reynolds number flow situations where the force dipole is the only contribution to hydrodynamic interactions.

First, numerical simulations of an isolated particle in a pure shear flow (far from any walls) were performed at different Reynolds numbers. The stresslet term represented by the symmetric part of the dipole tensor $\mathbf{G}$ was computed for particle Reynolds numbers up to 10 (the Reynolds number $Re_p = \frac{\gamma a^2}{\nu}$ is based on the shear rate, the particle radius and the fluid viscosity). Results are in very good agreement with those obtained by Mikulencak and Morris[20] from direct numerical simulations (see Figure 1 for the non-diagonal stresslet term G_{12}). The amplitude of normal stress differences (G_{11}–G_{22}) and (G_{22}–G_{33}) is an increasing function of the particle Reynolds number (see Figure 17 in the paper of Mikulencak and Morris[20]), suggesting that the suspension rheology could deviate from the Newtonian behavior when fluid inertia is finite. The agreement of our FCM simulations is also good for those quantities.

Second, the numerical method has been validated in the case of inertia-induced particle migration in a plane Poiseuille flow. In laminar channel flows, neutrally buoyant particles are submitted to a lift force induced by the interaction between the finite-size particle and the parabolic velocity profile when the particle Reynolds number is finite. The particles migrate towards an equilibrium position set by the balance between this lift force and the hydrodynamic wall repulsion (Segré-Silberberg effect). Many experimental and theoretical studies addressed this migration problem and they showed the existence of equilibrium positions that depend on the channel geometry, particle radius, and channel Reynolds numbers.[2,21,22] In Figure 2, the equilibrium position of a particle in

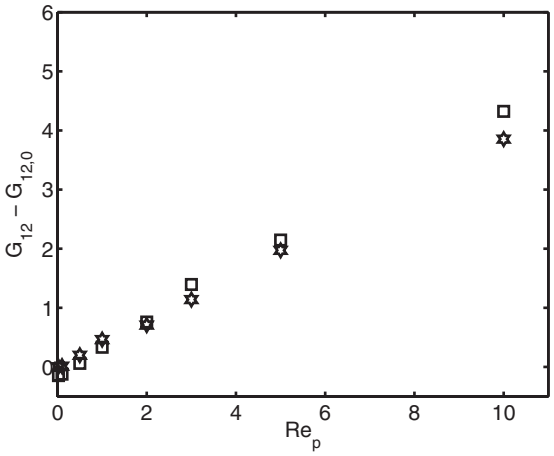

FIG. 1. Deviation of the non-diagonal stresslet term from the Stokes value (scaled by $\mu a^3 \gamma$) as a function of particulate Reynolds number $Re_p = \frac{\gamma a^2}{\nu}$. The □ and ⋆ symbols are, respectively, from FCM and DNS[20] simulations.

a plane Poiseuille flow is plotted versus the channel Reynolds number. The results obtained from the FCM simulations for $H/d = 16$ are compared to the prediction of Asmolov[23] based on matched asymptotic expansions. The FCM results shown here are obtained with a grid resolution of three grid points per particle radius and they show a good agreement with Asmolov's prediction (within a relative difference lower than 1.5%). Simulations with smaller particles (the size ratio was increased from $H/d = 16$ to $H/d = 20$ while the grid resolution per particle radius was kept constant) yielded unchanged particle equilibrium positions.

Additional simulations were carried to test the dependence of the results on the domain length and grid resolution. On one hand, simulations with box length equal to $14.4d$ and $28.8d$ (or in terms of the channel height $0.9H$ and $1.8H$, respectively) gave unchanged results on particle velocity and position evolution in time (for $Re = 100$ and 1500). On the other hand, the results on particle migration are slightly dependent on the grid resolution. When the mesh grid size was reduced from three to four grid points per particle radius, the strongest modification of the particle equilibrium

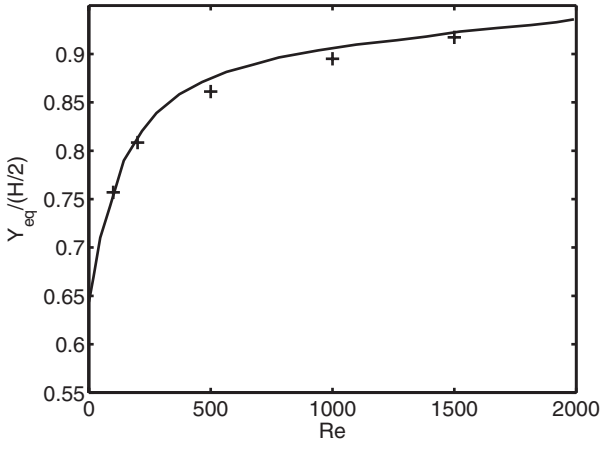

FIG. 2. Particle equilibrium position in a plane Poiseuille flow as a function of the Reynolds number. The solid line is the prediction obtained by Asmolov.[23] The plus signs are the FCM results. For this figure, $Y_{eq} = 0$ at the channel center and $H/2$ at the channel wall.

position occurred at $Re = 1500$. The distance between the channel wall and the particle equilibrium position is reduced from $1.5a$ to $1.3a$ with a smaller grid size.

Finally, we note that the agreement between the FCM results and the matched asymptotic expansions (for the particle migration results up to $Re = 1500$) is good. Hence, the finite-size particles considered in this paper are small enough so that the viscous effects are dominant at the particle scale while the inertial effects are not negligible far from the particle. However, as observed in Sec. V, the flow perturbations due to particle finite size are sufficiently large to modify the transitional flow structures.

III. SIMULATION PROCEDURE

A. Single-phase flows

Relaminarization of single phase flow is achieved by reducing progressively the Reynolds number until complete damping of the flow fluctuations. However, this procedure does not give a single value of the critical Reynolds number below which the turbulence vanishes. Instead, it gives information on the distribution of lifetime of a turbulent state. For example in pipe flows, the probability of lifetime follows a Poisson distribution.[24–26]

We carried out direct numerical simulations of single-phase flows in a plane channel, with periodic boundary conditions in streamwise and spanwise directions (x and z, respectively). No-slip boundary conditions are imposed at the channel walls (y is the wall-normal direction). Unlike fully turbulent and laminar flows, there is no straightforward relationship between the pressure-drop and the flow rate in the transition regime. Simulations at an imposed pressure-drop may induce undesired change of the average flow rate and hence Reynolds number in time. For this reason, in both single and two-phase flow cases, simulations were performed at a constant flow rate thanks to a regulation of the pressure-drop.

The distance between the channel walls is H, and the streamwise and spanwise lengths are πH. The velocity field is initialized with a laminar parabolic profile at $Re = 6000$ and a given amount of noise is added to initiate the transition to turbulence. The channel dimensions are sufficient to sustain turbulence in the sense that the domain size used is larger than the minimal channel at $Re = 6000$ (statistics were compared to the study by Jiménez and Moin[27]).

Most of the single-phase flow results shown in this paper are obtained using a mesh composed of 64^3 grid points, equally spaced in the homogeneous directions (corresponding to $\Delta x^+ = \Delta z^+ = 18.5$ at $Re = 6000$). In order to simulate precisely the small-scale vortices in the region very close to the channel wall and to minimize the number of grid points, hyperbolic tangent grid distribution is employed in the wall-normal direction following Moin and Kim.[28] We also carried out several simulations with a fine grid resolution ($256 \times 100 \times 256$ grid points corresponding to $\Delta x^+ = \Delta y^+ = \Delta z^+ = 4.6$ at $Re = 6000$). We observed minor impact of the grid size on the different flow fluctuation characteristics shown in this paper. The results which are the most influenced correspond to the r.m.s. of the vorticity fluctuations in the turbulent regime. Figures 3(a) and 3(b) show these profiles obtained from the coarse and fine grid simulations in turbulent ($Re = 6000$) and transitional ($Re = 1675$) flow cases. The spanwise component is barely influenced by the grid resolution in both flow regimes. While the wall-normal and the streamwise vorticity fluctuations are under-predicted by the coarse grid simulations in the fully turbulent regime, their dependence on the grid resolution is much weaker in the transition regime. We verified that other flow features obtained with the 64^3 mesh grid are correctly reproduced by simulations in the transition regime.

As Re is gradually decreased, the length of the coherent structures is increasing[29] until it eventually exceeds the length of the computational domain, requiring larger domains to fully capture the developed structures. However, the main objective of our study is to investigate the flow dynamics near the wall and further evaluate the effect of particles on that flow. For that purpose the size of the domain proposed is sufficient. For each new value of the Reynolds number, the computation time of simulations was set to $T_1 = 1000H/\langle U \rangle$, allowing the transition to a fully laminar regime to take place when occurring.

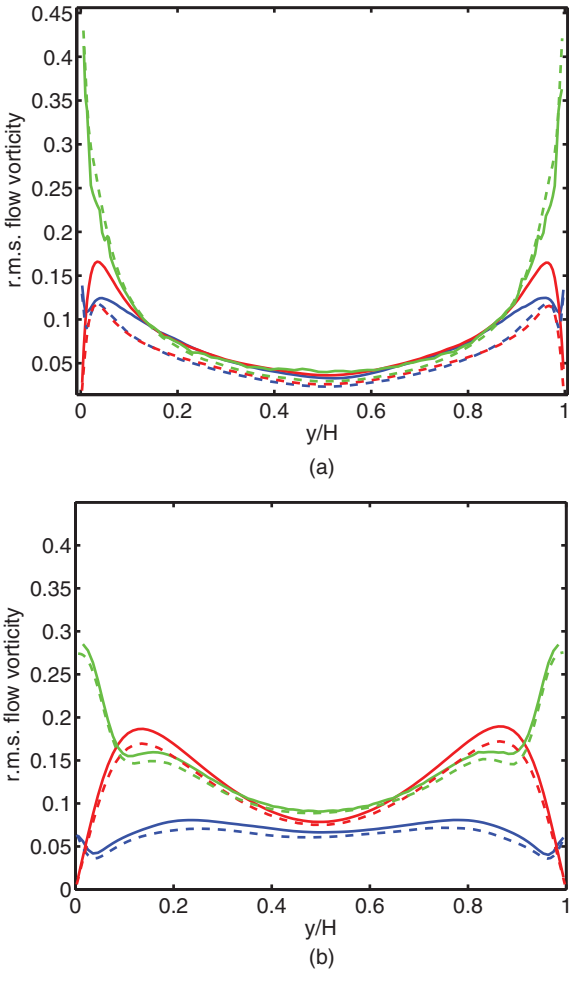

FIG. 3. Profiles of r.m.s. vorticity fluctuations at (a) $Re = 6000$ and (b) $Re = 1675$ scaled by u_τ^2/ν (solid lines stand for fine grid simulations while dashed lines stand for coarse grid simulations). Green color is for spanwise, red for wall-normal, and blue for streamwise components.

B. Two-phase flows

The particle size is chosen such that $H/d = 16$. This particle-to-channel size ratio is expected to sustain turbulence to a lower critical Reynolds than in single-phase flow, even at very low solid volume fractions.[9]

The particle-laden flow simulations require finer mesh grid compared to the single-phase flow simulations (three grid points per particle radius are used for the present simulations). Hence, the single-phase flow configuration (chosen as the initial condition for the two-phase flows) is linearly interpolated on a finer regular mesh grid ($320 \times 100 \times 256$ cells). As for the domain size, the distance between the walls and the streamwise length of the domain are kept H and πH, respectively, and the spanwise length is reduced to $2.5H$. The box truncation in the spanwise direction shifts the transition regime from $Re = [1600–1850]$ to $[1800–2000]$. This is the only effect we observed for the truncation operation for single phase flow dynamics.

The starting point for the computation of the suspension flow is one snapshot taken from the single-phase flow case at $Re = 1625$ (the lowest Reynolds number above which the flow remains fluctuant). Then 3107 particles are initially seeded at random positions in the simulation box, corresponding to a particle volumetric concentration $\phi = 5\%$. Then the relaminarization of the suspension flow is considered by reducing the Reynolds number (similar to the single-phase flow

TABLE I. Probability of relaminarization after two different simulation times $T_1 = 1000H/\langle U\rangle$ and $T_2 = T_1/3$.

Re	Probability of relaminarization before T_1	Probability of relaminarization before T_2
1850 → 1800	0%	0%
1800 → 1750	80%	0%
1750 → 1725	40%	0%
1725 → 1675	80%	40%
1675 → 1625	80%	40%
1625 → 1575	100%	100%

simulations). As the number of grid cells of the domain is greatly increased, each simulation of the suspension flow has been run during $T_2 = 800H/\langle U\rangle$ (taking 80 days parallel computation on 64 processors).

IV. SINGLE PHASE FLOW IN THE TRANSITION REGIME

Starting from $Re = 6000$, the Reynolds number has been progressively decreased in successive simulations until the flow became fully laminar. The Reynolds number was decreased from 6000 to 3000 with a step of 1000. Then it was decreased from 3000 to 2000 with a step of 200. Below $Re = 2000$, where the flow enters the transition regime, the step decay applied to the Reynolds number could have a significant impact on the flow evolution. The step value has to be small enough to prevent early turbulence extinction, and reasonably high in order to minimize the number of simulations. Hence in the transition regime, the Reynolds number was decreased by a step of 50 and five simulations were carried out for each Reynolds number, starting from different initial conditions (obtained from the simulations at previous Re). The flow became fully laminar for all five simulations at $Re = 1575$. Table I summarizes the number of cases that laminarized for each Reynolds number step decay within elapsed times T_1 and T_2.

A. Wall friction and velocity fluctuations

The wall friction coefficient and the velocity fluctuations were computed for each Reynolds number. The corresponding results are shown in Figure 4. Figure 4(a) shows good agreement between computed data and Dean's friction law for a smooth-wall flow. In the range of $Re = 2000$–5000, our numerical simulations slightly underestimate the value of the friction coefficient, probably because the mean velocity profile in the logarithmic region (not presented here) exhibits slightly larger values than the wall turbulent law. Such a discrepancy between the velocity profile in this range of Reynolds numbers and the fully turbulent profile has been confirmed earlier by Moser, Kim, Mansour.[30]

Contrarily to the evolution of the friction coefficient reported in previous studies on pipe and channel flows,[31–33] Figure 4(a) shows a sudden decrease at $Re = 1575$ of the friction coefficient, from the value corresponding to a turbulent regime to the value predicted analytically from a laminar plane Poiseuille flow. This abrupt change of the friction coefficient is due to the size of the domain used in the present work which is not long enough to allow an accurate description of the transition in "real channel flow" conditions, because it does not account for the coexistence of alternate laminar and fluctuating structures over large distances. Simulations (for the same conditions) with a double streamwise dimension ($2\pi H$ instead of πH) exhibited the same behavior. Hence, much longer channels should be considered to observe the progressive evolution of the friction coefficient from the turbulent to laminar law behavior as in the experiments. This will become quickly prohibitive for the simulation of particulate cases. However we consider that the box size used for the present simulations is suitable to reveal the important features related to the presence of particles in a transitional flow (fluid-particle interactions responsible of the sustainment or damping mechanisms).

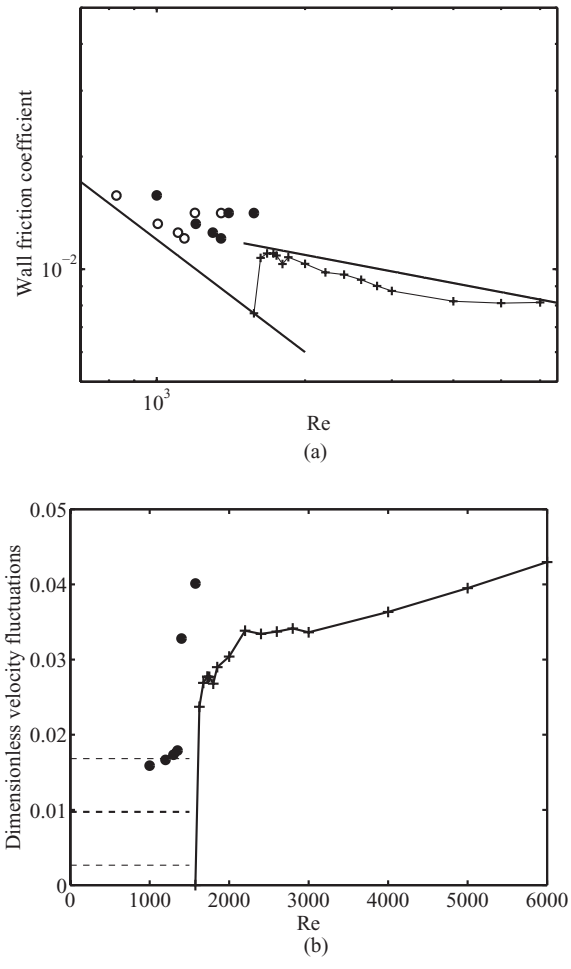

FIG. 4. (a) Wall friction coefficient and (b) dimensionless velocity fluctuations (Eq. (8)) versus Reynolds number. Symbols: +, single-phase flow and •, two-phase flow. (a) The solid lines represent the laminar law ($C_f = 12/Re$) and turbulent Dean's law for a smooth wall ($C_f = 0.073Re^{-1/4}$) for channel flows. The circle symbols, ○, are for friction coefficient of two-phase flows calculated with Reynolds numbers based on effective viscosity (Eq. (10)). (b) The solid line is only for eye guidance. Thick dashed line is the average particle shear-induced agitation calculated from (Eq. (11)) with the standard deviation underlined by thin dashed lines.

Figure 4(b) shows the evolution of the intensity of the transverse velocity fluctuations (Eq. (8)) as a function of Re:

$$I = \frac{\sqrt{0.5\left(\langle v'^2\rangle + \langle w'^2\rangle\right)}}{\langle U\rangle}, \tag{8}$$

where $\langle v'^2\rangle$ and $\langle w'^2\rangle$ are time and space-averaged velocity fluctuations, respectively, in the wall-normal and spanwise directions. The intensity of the velocity fluctuations barely decreases while the Reynolds number is reduced, before vanishing abruptly at $Re = 1575$.

The friction coefficient obtained by numerical simulations of turbulent single-phase flows oscillates around the time-average with an amplitude close to 20% of the average value. The characteristic oscillation timescale is of the order of $100H/\langle U\rangle$, in agreement with the observations of Jiménez and Moin.[27] However when the flow approaches relaminarization, the amplitude of the oscillations increases up to about 40% of the time-average value, without significant modification of the frequency. It is of particular interest to look in Figure 5 at the evolution of the wall friction coefficient at $Re = 1575$ immediately before relaminarization occurs. The temporal signal for the single-phase case (solid line) shows that the skin friction coefficient oscillates between a

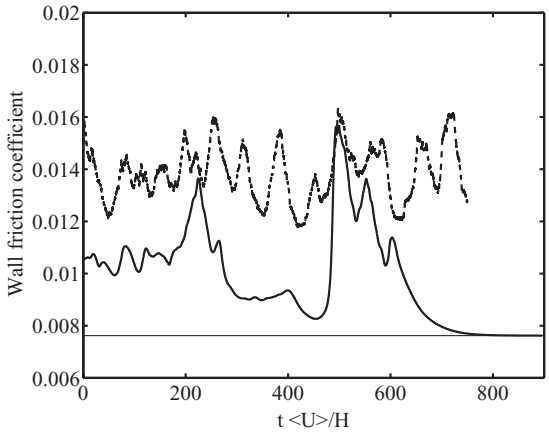

FIG. 5. Temporal evolution of the wall friction coefficient at $Re = 1575$. Solid line: single-phase flow. Dashed line: two-phase flow. Horizontal line: laminar regime value.

quasi-laminar state, where it is almost constant and close to the value corresponding to the laminar regime (horizontal line in Figure 5), and a turbulent state corresponding to a velocity profile almost fitting the standard logarithmic law. The intermittency of the flow at this critical Reynolds number (also noticed on the evolution of the flow velocity fluctuations in time) is consistent with the experimental observations[31] and direct numerical simulation results.[32]

B. Coherent structures prior to laminar state

The λ_2-criterion[34] has been used to educe the vortical structures in single-phase flows. These structures are plotted in Figure 6 just before the flow became laminar at $Re = 1575$. The size of the box seems to be appropriate as the developing elongated structures are slightly smaller than the length of the domain. Figure 6 suggests that the quasi-coherent streamwise vortices play an important role in the bursting phenomena that sustains the turbulence in the flow before laminar regime is reached. Vortical structures are distributed over the entire channel, and not concentrated in the near-wall region. The distribution, shape and size of the coherent structures are consistent with the conclusions of Iida and Nagano[32] on the relaminarization mechanisms. These authors have shown that while the quasi-laminar state appears, the viscous sub-layer thickness increases, leading to a shift in the maximum position of streamwise velocity fluctuations towards the channel center.

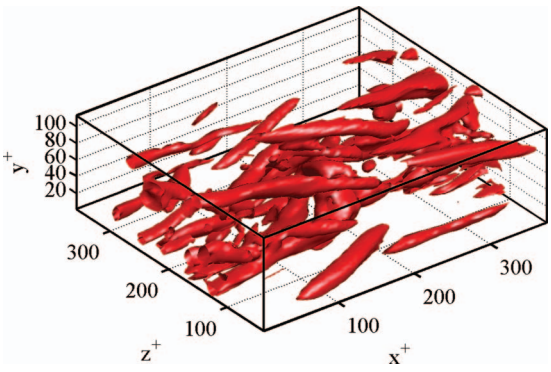

FIG. 6. Coherent structures visualized by the λ_2-criterion for the single-phase case at $Re = 1575$ before the flow relaminarizes. The magnitude of the contours shown here is equal to four times the standard deviation. Simulation domain is in wall units.

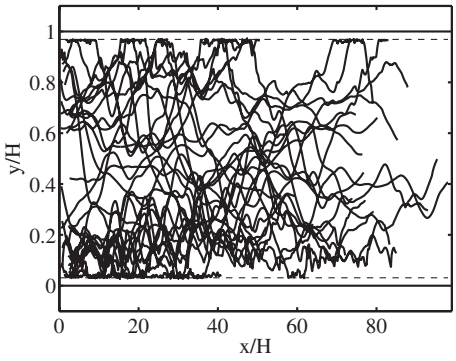

FIG. 7. Sample of particle trajectories projected in the mean-shear plane (xy) at $Re = 1575$. Horizontal solid lines indicate the wall locations. Horizontal dashed lines indicate the position of the particle center when the particle starts to overlap the wall.

V. FLUCTUATION ENHANCEMENT BY PARTICLES IN THE TRANSITION REGIME

Particles are randomly seeded in the unsteady channel flow before the flow completely relaminarizes at $Re = 1575$. In this range of flow Reynolds numbers, the particle Reynolds number, defined as $Re_p = \frac{\gamma a^2}{\nu}$ where γ is the local shear rate, is smaller or equal to 10, lying within the range of validity of the FCM method in a simple shear flow (see Figure 1).

At $Re = 1575$ where the single-phase flow fully relaminarizes, a turbulent-like behavior is maintained in the two-phase flow case. A sample of 30 particle trajectories is drawn in Figure 7 showing that they occupy all the flow region, whereas in a laminar flow, particles are expected to migrate towards the near-wall region (Segré-Silberberg effect, illustrated in Figure 2) and their deviation from the equilibrium positions results from multi-particle interactions due to the shear flow. While particle migration towards the channel walls is clearly observed in Figure 7, some particles in the near-wall region are pulled off by the turbulent structures occurring from bursting phenomena, to be transported again in the core region of the flow.

A. Average profiles of fluctuating suspension flows

The flow velocity, particle volume fraction and total shear stress profiles obtained from the two-phase flow simulations at $Re = 1575$ are plotted in Figures 8–10 and averages have been computed over the time and the homogeneous directions x and z.

A snapshot of particle centers in the (xy) plane is reported in the inset of Figure 8 (after steady state was reached), showing that particles occupy the entire domain, with a larger presence in the near-wall region. Indeed, the solid volume fraction profile confirms the homogeneity of the suspension: it is almost constant (ϕ slightly less than 5%) in the core of the channel, with a concentration peak ($\phi \approx 10\%$) near each wall due to particle migration across streamlines of the mean flow. The local minimum located near the peaks in the concentration profile is likely due to excluded volume effect (finite size of particles).

The suspension velocity profile (squares in Figure 9) suggests that the averaged suspension flow matches exactly the fluctuating single phase flow profile at same Reynolds number ($Re = 1575$). Moreover, the velocity profile in the transition regime is flatter than the laminar velocity profile in the channel core region, but it exhibits a lower velocity gradient at the channel walls than the fully turbulent velocity profile.

The total shear stress, (sum of viscous and Reynolds stress contributions) normalized by the wall shear stresses, is displayed in Figure 10 for both single and two-phase fluctuating flows. Both curves indicate that the macroscopic momentum balance corresponds to a steady parallel flow in both cases. The two-phase flow profile shows a bump near the walls, due to higher concentration and therefore to larger hydrodynamic interactions in that zone.

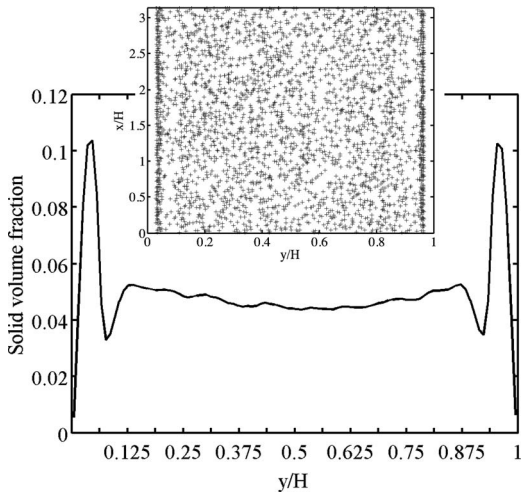

FIG. 8. Average particle volume fraction profile at $Re = 1575$. Inset: instantaneous projection of the particle centers in the mean-shear plane (xy).

B. Wall friction and velocity fluctuations

The presence of particles in the near-wall region increases the velocity fluctuations and the wall friction coefficient (Figure 4). The temporal evolution of the wall friction coefficient of the particulate flow at $Re = 1575$ is plotted in Figure 5. The friction coefficient is increased by a factor 1.5 compared to the single-phase case at same Reynolds number. Figure 5 suggests that intermittency revealed by the low-frequency high-amplitude fluctuations of the friction coefficient is sustained as in single-phase flows, with slightly higher oscillating frequency. It is probably due to the persistence of large-scale coherent structures of reduced size in the two-phase configuration, as suggested in Figure 12. Moreover, the temporal signal of the friction coefficient exhibits additional high frequency and small-amplitude fluctuations that are absent in the single-phase case. It is interesting to note that the time-scale of these small-scale fluctuations is a particle-induced time scale which order of magnitude is $O\left(a/\sqrt{\langle u'^2\rangle}\right)$, where $\sqrt{\langle u'^2\rangle}$ is the root mean square (r.m.s.) of velocity fluctuations in the flow direction. The time-averaged values of the friction coefficient in the suspension flow are reported in Figure 4(a) (black dots) for $1000 \leq Re \leq 1575$. The friction coefficient is larger than that predicted in either fully laminar or turbulent regimes. It is also nearly constant for $Re \geq 1400$,

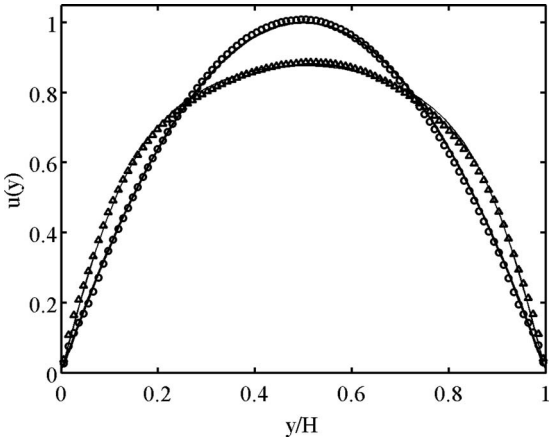

FIG. 9. Average velocity profiles of fluctuating flows at $Re = 1575$ (thin line for single phase flow and triangles for two-phase flow) and below the transition limit (solid line for single, i.e., Poiseuille flow, and circles for two-phase flow at $Re = 1200$).

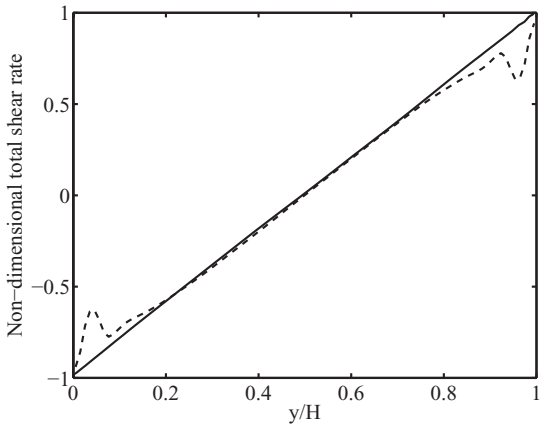

FIG. 10. Dimensionless shear stress profiles $\tau_{xy} = \left(\overline{u'v'} - \nu\overline{\partial U/\partial y}\right) / \left(\frac{1}{2} C_f \rho \langle U \rangle^2\right)$ at $Re = 1575$. Single-phase flow: solid line. Two-phase flow: dashed line.

indicating that the wall friction is mainly due to hydrodynamic interactions with a concentrated layer of particles close to each wall.

Normalized velocity r.m.s. profiles are shown in Figure 11 at $Re = 1575$. In single-phase flow at $Re = 6000$, data (not shown here) agree with those obtained both experimentally and numerically (Kim, Moin, Moser,[29] Moser, Kim, and Mansour[30]). In the transition regime, the single-phase flow profiles are modified with respect to the fully turbulent profiles, spanwise and wall-normal components reaching a maximum in the core of the channel instead of the near-wall region.

The r.m.s. velocity fluctuations calculated in the two-phase flow are obtained using a *composite-averaging* which does not distinguish the solid and fluid phases (as explained in Garcia-Villalba, Kidanemariam, and Uhlmann[13]). At this Reynolds number, the fluctuations in the flow direction are slightly altered by the particle presence, particularly in the center of the channel where particles tend to reduce large-scale structures induced velocity fluctuations. The effect of the particles is more significant for the wall-normal and spanwise fluctuating velocities. First, their intensity is nearly twice larger than the corresponding single-phase flow fluctuation level. Second, the profile shape

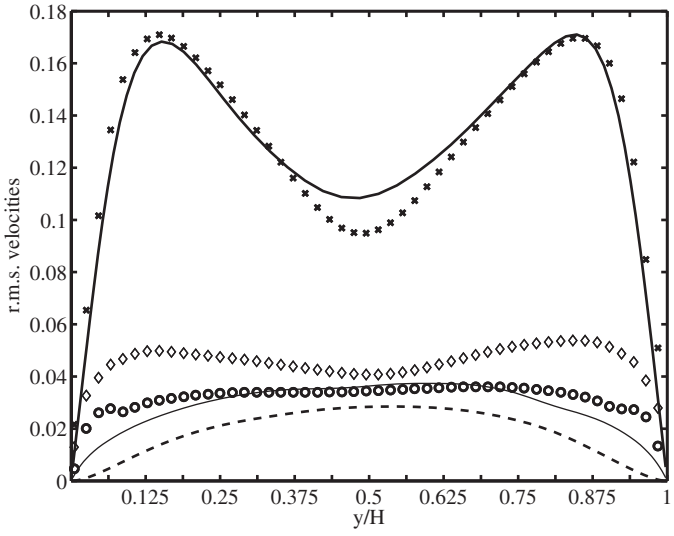

FIG. 11. Velocity component r.m.s. scaled by $\langle U \rangle$ at $Re = 1575$. Symbols are for two-phase flow profiles, in the flow ($\times$), wall normal ($\circ$), and spanwise ($\diamond$) directions. Lines are for single-phase flow simulations in the flow (solid), wall-normal (dashed), and spanwise (thin line) directions.

is quite different: it is almost flat in the channel core and stiffly decreases close to the walls. This behavior is opposite to the observations of Shao, Wu, and Yu[14] in turbulent flows at $Re = 5000$, $H/d = 10$, and $\phi = 7\%$. Their paper reported that particles increase the streamwise velocity fluctuations in the core of the channel, and slightly modify the wall-normal and spanwise fluctuation profiles compared to the single-phase turbulent flows. The difference between the turbulent and transitional fluctuation profiles of suspension flows seems to indicate that particles have different impact on the energy distribution in the system.

Note that the streamwise and spanwise profiles are slightly asymmetrical. Flows undergoing a laminar-turbulent transition are strongly unsteady. Hence, the asymmetry could be related to slightly unsteady statistics for the simulation time T_2. Another explanation is that the time-average particle number density is slightly larger in the lower part of the channel (0.3% of the total particle number), which might be related to the initial particle positions, since the preferential particle migration depends on the particle position relatively to the channel center.

The time and space-averaged transverse velocity fluctuations (Eq. (8)) at different Reynolds numbers are reported in Figure 4(b). The intensity of velocity fluctuations is increased compared to the single-phase case, due to the particle presence. Indeed, particles locally perturb the sheared fluid especially in the near-wall region where both the shear rate and the particle concentration are maximum. Particles also interact under the action of the large-scale flow structures. These hydrodynamic interactions increase the level of agitation in the channel flow.

2D snapshots of spanwise and streamwise vorticity fluctuations are displayed in Figure 12. Contour plots correspond to single-phase and two-phase flow patterns at the same Reynolds number $Re = 1575$ and in the range $[-\langle\gamma\rangle/2; \langle\gamma\rangle/2]$, where $\langle\gamma\rangle$ is the average shear rate of the single phase flow. Both spanwise and streamwise vorticity fluctuation fields of the single-phase flow let appear quasi-streamwise vortices stretching into the computational box. The diameter of the counter-rotating pair of structures extends over about a quarter of the domain width. We observe that the large-scale structures in transitional suspension flows are smaller, more numerous, and sustained down to lower Reynolds numbers than their counterpart in single-phase flows. During the relaminarization process of a single-phase flow, the characteristic size of the coherent structures expands, whereas the average intensity of the streamwise vorticity decreases. When the size of these rotational structures reaches the channel size, the flow is completely laminar. When adding particles, the delay of the relaminarization process seems to result from a resistance against the vortical structure expansion in favor of smaller structures, which have stronger rotational intensity.

Moreover, vorticity fluctuations in the vicinity of the particle surface and in the near-wall region are larger than anywhere else in the flow. This is mainly due to the interaction of the neutrally buoyant finite-size particles with the local shear rate (for example, in pure shear flow, at particle Reynolds numbers of order 5, the vorticity near the particle surface is 1.5 times larger than the average flow vorticity). Hence, Figure 12 suggests that the turbulence sustainment in particle-laden flow at $Re = 1575$ is both due to an additional source term of local perturbations induced by the particle finite size, and to the breakup of the large-scale eddies into smaller and more energetic vortical structures.

VI. SUSPENSION DYNAMICS BELOW THE TRANSITION

The Reynolds number of the suspension flow has been progressively decreased until relaminarization has been reached ($Re \leq 1350$). In the laminar regime, the average velocity profile of the suspension flow matches exactly the profile of a plane Poiseuille flow (Figure 9).

The time-averaged particle volume fraction profile is plotted in Figure 13 for $Re = 1200$. The concentration profile indicates two preferential particle positions due to lateral migration. They are located at a distance of one particle radius and four particle radius from the channel walls. The center of the channel is not completely depleted from particles as one may expect based on cross-stream migration of a single particle due to the Ségré-Silberberg effect.

Regarding the wall friction coefficient when the Reynolds number is decreased (black dots in Figure 4(a)), two different behaviors are suggested. For $Re = 1400$ and $Re = 1575$, the fluctuating flow undergoes nearly constant friction coefficient whereas the friction coefficient increases when

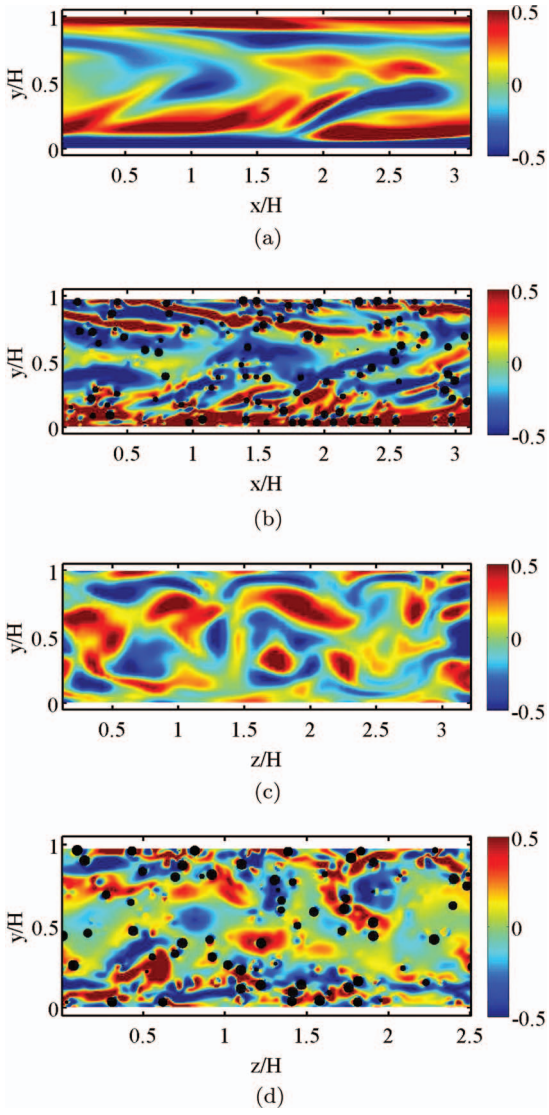

FIG. 12. 2D slices of ((a) and (b)) spanwise ω_z' and ((c) and (d)) streamwise ω_x' vorticity fluctuations at $Re = 1575$ in the median section of the simulation domain. The fluid is flowing from left to right in (a) and (b). (a)–(c) and (b)–(d) are for single and two-phase flows, respectively.

the Reynolds number is decreased below 1350. If the Reynolds number is replaced by a suspension effective viscosity based on Reynolds number, the black dots would be shifted to the open circle symbols in Figure 4(a). The suspension Reynolds number is defined by $Re_{eff} = \langle U \rangle H / \langle \nu_{eff} \rangle$ where the carrier fluid viscosity is replaced by a suspension average viscosity defined from the average shear stress in the channel such that

$$\left\langle \mu_{eff} \right\rangle \langle \gamma \rangle = \langle \mu_{sl}(y) \gamma_{sl}(y) \rangle \,, \tag{9}$$

where the brackets denote time and space averages in all directions, and the subscript sl refers to a suspension time-average performed only in the homogeneous directions (x and z). The local suspension viscosity depends on the local particle volumetric concentration and is evaluated from the model of Krieger and Dougherty[35] (Eq. (10)),

$$\frac{\mu_{sl}(y)}{\mu} = \left(1 - \frac{\phi(y)}{\phi_m}\right)^{-1.82} , \tag{10}$$

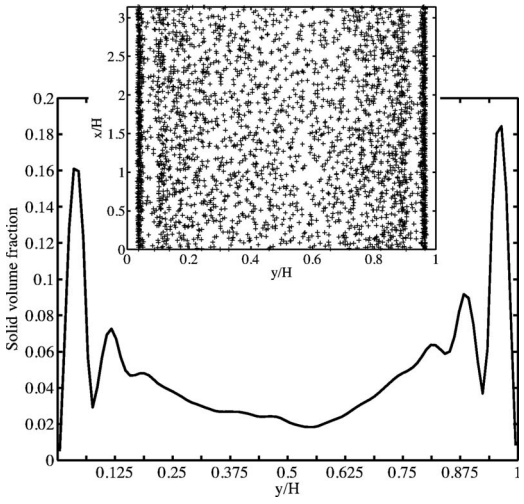

FIG. 13. Idem Figure 8 at $Re = 1200$.

where ϕ_m is the solid fraction at maximum packing ($\phi_m = 0.68$). When $Re \leq 1350$, if the carrier flow Reynolds number is replaced by the suspension Reynolds number Re_{eff}, the friction coefficient gets closer to the laminar single-phase law (open circles in Figure 4(a)).

Below 1350, averaged velocity fluctuations in the channel flow approach a minimum value, without dropping to zero as observed in the relaminarization process of the single-phase flow (Figure 4(b)). Plotting the temporal evolution of the average streamwise flow velocity fluctuation, Yu *et al.*[10] noted a threshold value between laminar and turbulent flow regime, which is of same order of magnitude as the minimum value observed in Figure 4(a) (direct quantitative comparison cannot be made due to difference in flow geometry and particle-to-pipe diameter ratio).

We estimated this minimum fluctuation level (thick dashed line in Figure 4(b)) from the shear-induced particle agitation predicted by the dilute limit in unbounded Stokes shear flow (Drazer *et al.*[3]). The shear-induced agitation depends on the local solid volume fraction and the local shear rate. Therefore, an average agitation in the channel flow is obtained from Eq. (11),

$$I_{shear} = \frac{\left\langle \sqrt{0.5\alpha\phi(y)\,[\gamma(y)a]^2} \right\rangle}{\langle U \rangle}, \tag{11}$$

where $\alpha = 0.4$ is a constant related to the dilute limit in Stokes flow, a is the particle radius. Since both the particle volume fraction ϕ and the shear rate γ strongly depend on the distance from the channel wall, the standard deviation of the shear-induced agitation across the channel is significant (represented by thin dashed lines in Figure 4(b)). The agitation due to transverse velocity fluctuations in the laminar suspension flow obtained by the numerical simulations falls within these bounds of shear-induced particle agitation.

VII. CONCLUSION

Direct numerical simulations have been carried out with single and two-phase channel flows in the transition regime, with the aim of understanding the effect of finite-size neutrally buoyant particles on the flow dynamics. The channel-to-particle size ratio $H/d = 16$ and the particle volumetric concentration $\phi = 5\%$ have been considered for this work.

In the transition regime, particles are homogeneously distributed throughout the channel, with concentration peaking in the near-wall region. Cross-stream migration of particles in channel flows occurs due to inertial lift force, resulting in an increase of the friction coefficient compared to the single-phase flow case at the same Reynolds number. The intensity of transverse velocity fluctuations is also found larger in particle-laden flow. Particles behave as a source of velocity perturbations in the

wall region leading to a significant enhancement of both the velocity fluctuations (in the wall-normal and spanwise directions) and the wall friction coefficient. On the contrary, streamwise velocity fluctuations are damped by the particles in the core region. Additionally, the impact of the particles on the vortical structures sustaining the turbulence has been investigated. It emerges from this study that particles break down the large-scale structures into smaller, more numerous, and more energetic eddies. The present results suggest that the interactions between particles and the large flow structures could be a possible reason for the decrease of the critical Reynolds number (below which the flow becomes fully laminar).

Once the turbulence is extinguished, particles migrate progressively towards the channel walls. The average velocity profile of the laminar suspension is not drastically modified by the non-homogeneous particle distribution. The average velocity fluctuations do not drop to zero in the laminar suspensions as for single-phase flows. Instead, they approach the average shear-induced agitation calculated from the limit of unbounded sheared suspension under Stokes flow approximation. The friction coefficient follows the friction coefficient law in a laminar single-phase channel flow provided that the Reynolds number is replaced by the effective suspension Reynolds number.

ACKNOWLEDGMENTS

This work was granted access to the HPC resources of CALMIP and GENCI under the allocations 2012-P1002 and x20132a6942, respectively. The authors would like to thank K. M. Yeo and M. R. Maxey for helpful discussions on the numerical method and A. Pedrono for technical support.

[1] G. Ségré and A. Silberberg, "Behavior of macroscopic rigid spheres in Poiseuille flow. Part I. Determination of local concentration by statistical analysis of particle passages through crossed light beams," J. Fluid Mech. **14**, 115–135 (1962).
[2] J. Schonberg and E. Hinch, "Inertial migration of a sphere in Poiseuille flow," J. Fluid Mech. **203**, 517–524 (1989).
[3] G. Drazer, J. Koplik, B. Khusid, and A. Acrivos, "Microstructure and velocity fluctuations in sheared suspensions," J. Fluid Mech. **511**, 237–263 (2004).
[4] M. Abbas, E. Climent, O. Simonin, and M. R. Maxey, "Dynamics of bidisperse suspensions under Stokes flows: Linear shear flow and sedimentation," Phys. Fluids **18**, 121504 (2006).
[5] D. Semwogerere, J. Morris, and E. Weeks, "Development of particle migration in pressure-driven flow of a Brownian suspension," J. Fluid Mech. **581**, 437–451 (2007).
[6] K. Yeo and M. Maxey, "Numerical simulations of concentrated suspensions of monodisperse particles in a Poiseuille flow," J. Fluid Mech. **682**, 491–518 (2011).
[7] M. Han, C. Kim, M. Kim, and S. Lee, "Particle migration in tube flow of suspensions," J. Rheol. **43**(5), 1157–1174 (1999).
[8] S. Balachandar and J. K. Eaton, "Turbulent dispersed multiphase flow," Annu. Rev. Fluid Mech. **42**, 111–133 (2010).
[9] J.-P. Matas, J. F. Morris, and E. Guazzelli, "Transition to turbulence in particulate pipe flow," Phys. Rev. Lett. **90**, 014501 (2003).
[10] Z. Yu, T. Wu, X. Shao, and J. Lin, "Numerical studies of the effects of large neutrally buoyant particles on the flow instability and transition to turbulence in pipe flow," Phys. Fluids **25**, 043305 (2013).
[11] Y. Pan and S. Banerjee, "Numerical investigation of the effects of large particles on wall-turbulence," Phys. Fluids **9**(12), 3786–3807 (1997).
[12] M. Uhlmann, "Interface-resolved direct numerical simulation of vertical particulate channel flow in the turbulent regime," Phys. Fluids **20**, 053305 (2008).
[13] M. García-Villalba, A. Kidanemariam, and M. Uhlmann, "DNS of vertical plane channel flow with finite-size particles: Voronoi analysis, acceleration statistics and particle-conditioned averaging," Int. J. Multiphase Flow **46**, 54–74 (2012).
[14] X. Shao, T. Wu, and Z. Yu, "Fully resolved numerical simulation of particle-laden turbulent flow in a horizontal channel at a low Reynolds number," J. Fluid Mech. **693**, 319–344 (2012).
[15] A. Kidanemariam, C. Chan-Braun, T. Doychev, and M. Uhlmann, "Direct numerical simulation of horizontal open channel flow with finite-size, heavy particles at low solid volume fraction," New J. Phys. **15**, 025031 (2013).
[16] I. Calmet and J. Magnaudet, "Large-eddy simulation of high-Schmidt number mass transfer in a turbulent channel flow," Phys. Fluids **9**, 438–455 (1997).
[17] M. R. Maxey and B. K. Patel, "Localized force representations for particles sedimenting in Stokes flow," Int. J. Multiphase Flow **27**, 1603–1626 (2001).
[18] S. Lomholt and M. R. Maxey, "Force-coupling method for particulate two-phase flow: Stokes flow," J. Comput. Phys. **184**, 381–405 (2003).
[19] E. Climent and M. Maxey, *The Force Coupling Method: A Flexible Approach for the Simulation of Particulate Flows* (Ressign Press, 2009).
[20] D. R. Mikulencak and J. F. Morris, "Stationary shear flow around fixed and free bodies at finite Reynolds number," J. Fluid Mech. **520**, 215–242 (2004).
[21] B. Ho and G. Leal, "Inertial migration of rigid spheres in two-dimensional unidirectional flows," J. Fluid Mech. **65**, 365–400 (1974).

[22] J.-P. Matas, J. F. Morris, and E. Guazzelli, "Lateral force on a rigid sphere in large-inertia laminar pipe flow," J. Fluid Mech. **621**, 59–67 (2009).
[23] E.-S. Asmolov, "The inertial lift on a spherical particle in a plane Poiseuille flow at large channel Reynolds number," J. Fluid Mech. **381**, 63–87 (1999).
[24] H. Faisst and B. Eckhardt, "Traveling waves in pipe flow," Phys. Rev. Lett. **91**, 224502 (2003).
[25] T. Mullin and J. Peixinho, "Transition to turbulence pipe flow," J. Low Temp. Phys. **145**, 75–88 (2006).
[26] M. Avila, A. Willis, and B. Hof, "On the transient nature of localized pipe flow turbulence," J. Fluid Mech. **646**, 127–136 (2010).
[27] J. Jiménez and P. Moin, "The minimal flow unit in near-wall turbulence," J. Fluid Mech. **225**, 213–240 (1991).
[28] P. Moin and J. Kim, "Numerical investigation of turbulence channel flow," J. Fluid Mech. **118**, 341–377 (1982).
[29] J. Kim, P. Moin, and R. Moser, "Turbulence statistics in fully developed channel flow at low Reynolds number," J. Fluid Mech. **177**, 133–166 (1987).
[30] R. Moser, J. Kim, and N. Mansour, "Direct numerical simulation of turbulent channel flow up to $re_\tau = 590$," Phys. Fluids **11**, 943–945 (1999).
[31] V. C. Patel and M. R. Head, "Some observations on skin friction and velocity profiles in fully developed pipe and channel flows," J. Fluid Mech. **38**, 181–201 (1969).
[32] O. Iida and Y. Nagano, "The relaminarization mechanisms of turbulent channel flow at low Reynolds numbers," Flow, Turbul. Combust. **60**, 193–213 (1998).
[33] V. Priymak and T. Miyazaki, "Direct numerical simulation of equilibrium spatially localized structures in pipe flow," Phys. Fluids **16**, 4221–4234 (2004).
[34] J. Jeong and F. Hussain, "On the identification of a vortex," J. Fluid Mech. **285**, 69–94 (1995).
[35] I. M. Krieger and T. J. Dougherty, "A mechanism for non-Nestonian flow in suspensions of rigid spheres," Trans. Soc. Rheol. **3**, 137–152 (1959).